Cell. Mol. Biol. (ISSN: 1165-158X)

Journal Homepage: www.cellmolbiol.org

Cellular and Molecular Biology

Original Article

Identifying a novel class of lead compounds for monoacylglycerol lipase inhibition: an integrated computational study

Faizul Azam*

Department of Medicinal Chemistry and Pharmacognosy, College of Pharmacy,Qassim University, Buraydah 51452, Saudi Arabia

Article Info

Article history:

Received: February 15, 2025
Accepted: April 05, 2025
Published: May 31, 2025

Use your device to scan and read the article online

Abstract

Monoacylglycerol lipase (MAGL) is a serine hydrolase that degrades the endocannabinoid 2-arachidonoylglycerol and other monoacylglycerols in the brain and peripheral tissues. Elevated MAGL levels in invasive malignancies promote tumor growth by releasing free fatty acids, making MAGL inhibition a potential strategy for treating cancer. In this study, a virtual screening workflow began with Pharmit web server, where a pharmacophore was generated based on the X-ray crystal structure of MAGL complexed with its inhibitor, (2-cyclohexyl-1,3-benzoxazol-6-yl){3-[4-(pyrimidin-2-yl)piperazin-1-yl]azetidin-1-yl}methanone. A total of 5.241 million molecules from the MolPort database were screened, utilizing its diverse and purchasable chemical space to enhance the likelihood of identifying novel MAGL inhibitors and facilitating experimental validation. After applying filters based on Lipinski's and Veber's rules, a maximum energy cutoff of -7.0 kcal/mol, and an RMSD of 2Å, 4027 hits were obtained. The compounds were then docked using Vina-GPU, and the top five hits, along with the co-crystal inhibitor, were further analyzed through DFT computations and molecular dynamics simulations. MMGBSA computations identified MolPort-007-806-063 as the most potent compound, with a binding energy of -59.9±0.23 kcal/mol. In comparison, the co-crystal inhibitor exhibited a binding energy of -56.26±0.22 kcal/mol, while the other compounds showed energies of -54.57±0.26 kcal/mol, -53.57±0.24 kcal/mol, -41.13±0.33 kcal/mol, and -36.23±0.36 kcal/mol. These compounds are promising MAGL inhibitor candidates for experimental validation through enzyme inhibition assays, cell-based activity assays, and crystallographic studies to confirm their predicted binding modes and potency.

Keywords: Anticancer treatment, MMGBSA, Molecular dynamics, Vina-GPU, Virtual screening.

1. Introduction

Over many decades of intensive research, a variety of anticancer compounds have been developed, leading to significant advancements in treatment options [1]. Despite these breakthroughs, cancer remains a formidable challenge in modern medicine. Many existing therapies, while beneficial, often fall short due to issues such as drug resistance, limited efficacy, and undesirable side effects [2]. This underscores the urgent and ongoing need for novel anticancer drugs that are not only more effective but also possess lower toxicity, improving both patient outcomes and quality of life. The development of innovative therapies that can target cancer cells with high precision while minimizing damage to healthy tissues is critical to addressing this unmet medical need [3].

Monoacylglycerol lipase (MAGL) is an essential serine hydrolase enzyme that catalyzes the breakdown of the endocannabinoid 2-arachidonoylglycerol (2-AG) and other monoacylglycerols, playing a key role in lipid metabolism within both the brain and peripheral tissues [4, 5]. By regulating the levels of 2-AG, MAGL influences many signaling pathways associated with cell growth, inflammation, and cellular homeostasis [6]. In general, aggressive tumors exhibit increased MAGL expression, which is known to facilitate tumor growth by releasing free fatty acids that enhance cancer cell proliferation and foster a malignant environment [7]. Thus, blocking MAGL offers a viable therapeutic approach, as it may impede cancer progression by modifying lipid signaling and decreasing the availability of fatty acids [8].

Recently, MAGL inhibitors have gained considerable attention for their potential role in cancer treatment [9, 10]. Among them, the compound JZL184 has demonstrated promising anticancer activity by inhibiting MAGL. This inhibition leads to an accumulation of the endocannabinoid 2-AG, which subsequently activates the CB1 cannabinoid receptor. This receptor activation initiates notable antimetastatic and anti-invasive effects, particularly observed in lung cancer cells [11]. In another investigation, treatment of colorectal cancer cell lines with JZL184 resulted in reduced tumor growth, enhanced apoptosis, and improved sensitivity of tumor cells to 5-fluorouracil [12]. Furthermore, studies have shown that the reversible MAGL inhibitor 1,5-diphenylpyrazole-3-carboxamide exhibits antiproliferative properties on cancer cell lines and alleviates oxaliplatin-induced neuropathic

* Corresponding author.
E-mail address: f.azam@qu.edu.sa (F.Azam).
Doi: http://dx.doi.org/10.14715/cmb/2025.71.5.14

hypersensitivity in vivo [13]. Compound 23 significantly reduced the viability of breast, colon, and ovarian cancer cell lines, exhibiting IC50 values in the low micromolar range. However, its potential was limited by inadequate solubility [14]. These findings hold substantial promise for the future of cancer research, suggesting that selectively targeting MAGL could complement or even surpass current treatment strategies by halting tumor progression at the metabolic level. By impeding fatty acid release and modulating endocannabinoid signaling, MAGL inhibitors have the potential to reduce both tumor proliferation and metastasis while enhancing the effectiveness of existing chemotherapeutics.

Computer-aided drug design (CADD) has become indispensable in modern drug discovery, offering precision and efficiency in identifying and optimizing lead compounds [15]. Techniques like pharmacophore modeling enable researchers to define essential molecular features for bioactivity, guiding the design of potent compounds. Virtual screening further accelerates the discovery process by sifting through large compound libraries to pinpoint promising candidates [16]. Molecular dynamics (MD) simulations provide insights into protein-ligand interactions at an atomic level, enhancing our understanding of stability and binding modes. Quantum-based methods such as density functional theory (DFT) allow detailed examination of electronic properties, while molecular mechanics with generalized born surface area (MM/GBSA) calculations offer accurate binding energy estimations, refining lead optimization [17, 18]. Together, these CADD techniques are reshaping the drug discovery landscape, making the process more targeted and resource-efficient. These computational workflows (Fig. 1) used in this study lay the groundwork for more advanced in vitro and in vivo validations, ultimately shaping a new generation of targeted therapies aimed at minimizing toxicity and resistance. In the broader vision of this study, the integration of CADD with other cutting-edge approaches will further refine drug candidate design, streamline the discovery process, and accelerate the translation of these novel MAGL inhibitors into clinically viable anticancer treatments, thereby improving patient outcomes and long-term quality of life.

2. Materials and methods

2.1. Virtual screening

The Pharmit [19] web server was utilized to create pharmacophore model based on the X-ray crystal structure of the inhibitor ZYH bound to the MAGL protein, with PDB ID 3PE6. After evaluating multiple protein structures, this protein was selected for its 1.35 Å resolution, low R-value of 0.147, minimal missing residues, and its origin from *Homo sapiens*. The selection criteria prioritized high resolution, low R-values, and minimal missing residues to ensure comprehensive coverage of the binding site. Additionally, a protein co-crystallized with an inhibitor was preferred to facilitate the identification of binding pocket residues for virtual screening and docking.

The pharmacophore model was then employed for virtual screening against the MolPort database, which includes 5.241 million molecules. To ensure that only compounds with favorable properties progressed through the screening process, multiple filtering criteria were applied. The pharmacophore shape filter was used to capture the essential three-dimensional features required for target binding, thereby enhancing the likelihood of identifying active compounds. Lipinski's "rule of five" [20] was incorporated to filter out molecules that are unlikely to be orally active, by limiting molecular weight to ≤500, logP to ≤5, hydrogen bond acceptors to ≤10, and hydrogen bond donors to ≤5, which together serve as indicators of good absorption and permeability. In addition, Veber's filter [21] was implemented by restricting the number of rotatable bonds to ≤10 and the polar surface area to ≤140 $Å^2$, parameters that correlate with improved oral bioavailability and conformational stability. An energy cutoff of -7.0 kcal/mol was set to exclude less energetically favorable interactions, while a minimized RMSD (mRMSD) cutoff of 2 Å was applied to ensure that the predicted binding poses remained consistent with the initial query-aligned conformation after energy minimization [22].

2.2. Molecular docking by Vina-GPU

Gypsum-DL 1.2.1 [23] was employed to generate 3D models of filtered molecules in SDF format. Additionally, the durrant_lab_filters flag was applied to refine the models to eliminate variants that, while chemically feasible, are unlikely according to Durrant lab standards. Ultimately, 4,027 processed molecules were saved individually in PDB format, which was subsequently converted to PDBQT format using Open Babel 3.1.1 [24].

AutoDock Vina-GPU 2.1 [25, 26] was then used for molecular docking of the 4,027 molecules to the MAGL protein in a single run. The GPU-accelerated platform significantly enhanced docking speed and accuracy, which is crucial for rapid drug discovery. Each compound required approximately one second for docking. AutoDock Vina-GPU 2.1 was installed on a Linux workstation running Rocky Linux 9, equipped with a 24-core AMD Ryzen AM4 4.8 GHz processor, a 12 GB NVIDIA GeForce RTX 3080 Ti Trinity GPU, 64 GB DDR4 C18 AMD RAM, and an NVMe hard disk.

The docking process centered on the binding site of the co-crystallized ligand, ZYH [27], with a grid box positioned at coordinates -10.87, 20.029, and -9.412 (x, y, and z axes) and a dimension of 30 points in each direction. The default thread size was set to 8000 [25]. Following the docking, an in-house Python script was used to analyze and rank the binding energies of each model, organizing the output files for detailed assessment of docking results.

2.3. Molecular dynamics

To replicate the cellular conditions in silico, complexes

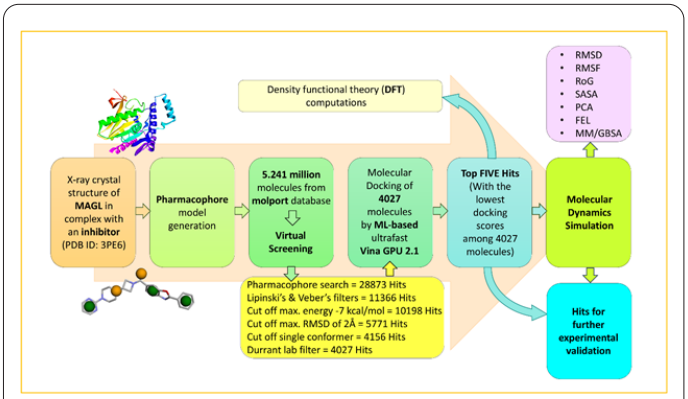

Fig. 1. A schematic flowchart illustrates the steps followed in this study.

of selected molecules and the ZYH-bound MAGL protein underwent comprehensive all-atom molecular dynamics (MD) simulations using GROMACS version 2022.3 [28]. Briefly, protein-ligand complexes were placed in cubic simulation boxes filled with TIP3P water, neutralized and balanced with Na^+ and Cl^- ions. MAGL was parameterized using AMBER99SB-ILDN whereas ligands were treated with GAFF2 force fields. Energy minimization was performed using the steepest descent algorithm, and systems underwent 1 ns equilibration under NVT and NPT ensembles. Finally, the production simulations were performed for 100 ns in the NPT ensemble.

2.4. MMGBSA binding free energy calculations

Binding free energies for ligands were computed using the MMGBSA method with the gmx_MMPBSA tool [29]. To ensure metastable sampling for analysis, a total of 200 frames were collected at intervals of 0.1 ns from the final 20 ns of MD simulations. The binding energy calculations included gas-phase (electrostatic and van der Waals) and solvation (polar and nonpolar) energy contributions. Additionally, per-residue energy contributions were analyzed to understand ligand-receptor interactions [30].

2.5. DFT computations

Density functional theory (DFT) calculations were carried out using the Orca 5.0.4 software package [31]. Geometry optimizations for the compounds were performed with the 6-311G(d,p) basis set, employing the Lee-Yang-Parr correlation functional (B3LYP) [32, 33]. The highest occupied molecular orbital (HOMO) and the lowest unoccupied molecular orbital (LUMO) were visualized through the Avogadro program (http://avogadro.cc/).

3. Results

3.1. Virtual screening and molecular docking by ML-based ultra-fast Vina-GPU

The virtual screening process aimed at identifying inhibitors of MAGL is outlined in Figure 1. A pharmacophore model was developed on the Pharmit web server, utilizing a bound inhibitor from the X-ray crystal structure of MAGL (PDB ID: 3PE6). This pharmacophore successfully captured essential chemical and spatial features necessary for ligand binding to MAGL, based on the interactions of (2-cyclohexyl-1,3-benzoxazol-6-yl){3-[4-(pyrimidin-2-yl)piperazin-1-yl]azetidin-1-yl}methanone with the enzyme. The pharmacophore model served as a shape filter to virtually screen a library of 5.241 million molecules from the Molport database, identifying an initial set of 28,873 hits.

Subsequent filtering using Lipinski's rule of five and Veber's rule reduced the number of hits to 11,366. Energy minimization was then performed using AutoDock Vina and Smina on the Pharmit server, applying a binding affinity cutoff of -7.0 kcal/mol, resulting in 10,198 molecules. Structural alignment using root mean square deviation (RMSD) filtering removed molecules with deviations above 2Å, leaving 5,771 compounds. A single conformer stability filter further refined the hits to 4,156 molecules. Next, the Gypsum-DL program generated 3D models from 2D structures, and the Durrant lab filter excluded problematic molecules, leaving 4,027 candidates. These were docked using Vina GPU-2.1, and the top five scoring molecules were selected for subsequent molecular dynamics (MD) simulations.

3.2. Molecular docking

AutoDock Vina-GPU 2.1 was employed to dock 4027 compounds obtained from virtual screening into the active site of MAGL. This software employs thousands of GPU cores for parallel processing, allowing it to perform docking operations at a rate of up to 50 times faster while maintaining the same level of accuracy. The results are summarized in Table S1 of supplementary information. Out of these, the top five ligands showing the highest docking score were selected to further analysis by MD simulation. The intermolecular interactions of these ligands along with co-crystallized inhibitor of MAGL which serves as control, are presented in Fig. S1 of supplementary information.

Across all compounds shown in Figure S1, consistent hydrogen bonding interactions are observed with residues like Ala51, Met123 and Ser122, which play a pivotal role in stabilizing the ligand within the binding pocket. Hydrophobic contacts with residues such as Leu213, Leu241, and Val270 further enhance ligand binding, forming a hydrophobic environment that anchors the ligand. π-π stacking interactions, notably with Tyr194, add another layer of stabilization through aromatic interactions. Moreover, it also contributes to establishing polar contacts with compounds Molport-010-716-199, Molport-020-263-494 and MolPort-007-806-063. An additional hydrogen bond was also formed between Glu53 and Molport-010-716-199. These analyses could guide future ligand optimization for improved binding affinity and efficacy.

3.3. Molecular Dynamics

3.3.1. Root-mean square deviation (RMSD)

The RMSD plot indicates that all six complexes, including the control, exhibit overall stability throughout the 100-nanosecond simulation. This is evident from the RMSD values remaining within a reasonable range-typically between 1.0 Å and 3.0 Å-with average values not

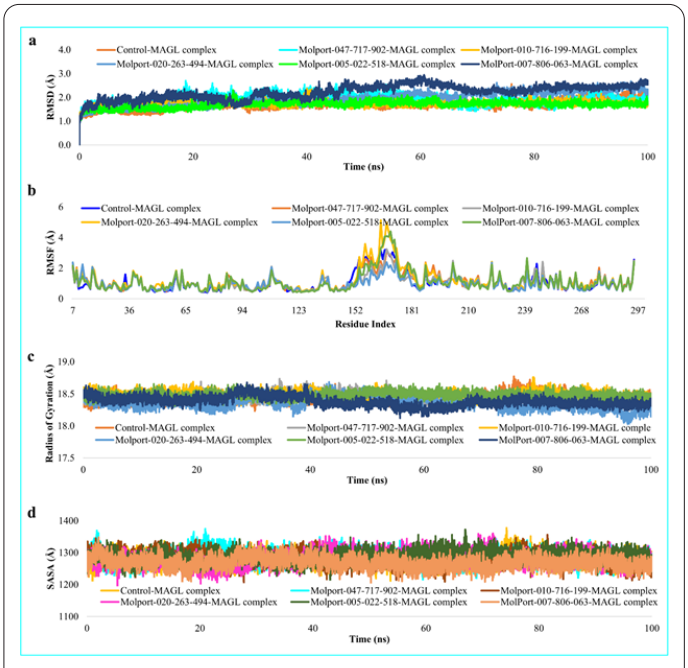

Fig. 2. Results of molecular dynamics in terms of root mean square deviation (a), root mean square fluctuation (b), radius of gyration (c) and solvent accessible surface area (d) for the top five hits along with native inhibitor.

exceeding 2.2 Å in any complex. While initial interactions caused minor deviations, the ligand-protein complexes eventually stabilized over time (Figure 2a).

3.3.2. Root-mean square fluctuation (RMSF)

Figure 2(b) presents the RMSF plots of six ligand-MAGL complexes, including the control. The analysis of the peaks indicates that all structures remain stable throughout the simulation, with no major deviations observed. Most residues exhibit fluctuations below 3 Å, reflecting minimal structural changes. A prominent increase in flexibility is observed around residues 150-190 across all complexes, likely due to inherent flexibility or ligand interaction, while the rest of the enzyme remains stable. Ligands such as Molport-005-022-518 and Molport-010-716-199 exhibit RMSF profiles comparable to the control, indicating their minimal impact on residue flexibility. Although Molport-020-263-494 and Molport-047-717-902 exhibit slightly higher fluctuations, these complexes remain stable overall.

3.3.3. Radius of gyration

The radius of gyration (Rg) is a measure of the compactness of a protein structure, with lower values indicating a more compact and stable conformation and higher values suggesting expansion or flexibility. During the 100-nanosecond simulation of the six ligand-MAGL complexes, the Rg values change only slightly (17.6 Å to 18.8 Å), which means that all structures stay stable and compact. The control complex maintains consistent Rg values around 18.2 Å, serving as a reliable baseline. Ligands like Molport-007-806-063 slightly lower the Rg, which points to a more compact shape. On the other hand, Molport-010-716-199 and Molport-047-717-902 show small changes, which account to some flexibility (Fig. 2c).

3.3.4. Solvent accessible surface area

Understanding ligand-protein interactions depends greatly on solvent-accessible surface area (SASA), which measures the amount of protein surface exposed to the surrounding solvent. Changes in SASA can signal shifts in protein conformation, ligand binding, or interactions with the solvent, offering insights into the stability and dynamics of the complex. Fig. 2(d) displays the SASA results for the virtually screened molecules in complex with MAGL. The average SASA values range from 1270 Å^2 to 1289 Å^2. The peaks indicate consistent solvent exposure across all complexes, suggesting steady interactions throughout the simulation. In particular, Molport-007-806-063 has the lowest average SASA value at 1270 Å^2, suggesting a tighter interaction with the enzyme due to a more compact shape. On the other hand, Molport-005-022-518 has the highest SASA at 1289 Å^2, indicating slightly more solvent exposure, which could reflect minor flexibility in the binding region. However, this small difference does not point to any significant changes or instability in the interaction.

3.3.5. Hydrogen bond analysis

The hydrogen bond analysis highlights distinct interaction patterns across the MAGL-ligand complexes. Molport-007-806-063 always makes two to three hydrogen bonds with the protein during the simulation. This shows that it binds strongly and reliably, which is in line with its high binding affinity. In contrast, Molport-010-716-199 demonstrates more fluctuating behavior, forming between 1 and 5 bonds, suggesting a flexible binding mode that adapts dynamically during the simulation. Similarly, Molport-047-717-902 shows variability in its hydrogen bond interactions, ranging from 1 to 4 bonds, reflecting transient but occasionally strong interactions with the protein. On the other hand, Molport-005-022-518 and Molport-020-263-494 maintain fewer hydrogen bonds, typically between 1 and 2. A moderate number of hydrogen bonds are formed by the control ligand, ranging from 1 to 2 bonds (Fig. 3).

3.3.6. Free energy landscapes (FEL) analysis

Gibbs free energy landscapes (FEL) offer valuable insights into the stability and conformational dynamics of protein-ligand interactions by plotting structural parameters, such as the Rg and RMSD, against Gibbs free energy. The FEL plots for the control and the five hit ligands in complex with MAGL indicate that all systems exhibit stable binding, as evidenced by the presence of deep energy wells, signifying energetically favorable conformations (Fig. 4a-f). Among the ligands, Molport-007-806-063 stands out with the deepest well, indicating a highly stable and compact conformation, which aligns with its strong binding affinity. Similarly, Molport-010-716-199 and Molport-005-022-518 display favorable stability profiles, maintaining compact structures throughout the simulation, and suggesting strong interactions. In contrast, Molport-047-717-902 and Molport-020-263-494 exhibit slightly elevated Rg values, implying that these ligands induce more flexibility within the binding pocket, although they still demonstrate overall structural stability. The FEL data highlights the different degrees of stability and compactness induced by the ligands, with Molport-007-806-063 showing the most robust interaction.

3.3.7. Principal component analysis (PCA)

Principal component analysis (PCA) is a powerful tool in MD simulations for identifying the dominant motions and conformational transitions in protein-ligand complexes. The PCA plots for the control and five hits in complex with MAGL show distinct patterns of conformational flexibility and stability. The control, along with Molport-010-716-199 and Molport-007-806-063, exhibits two clear conformational clusters, suggesting that these systems dynamically transition between two stable states (Fig. 4g-l). This indicates that while the systems are flexible,

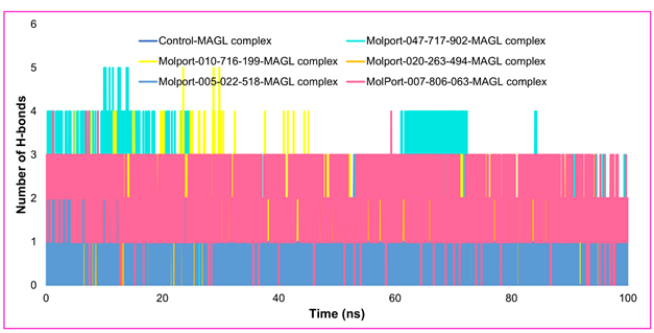

Fig. 3. Results of molecular dynamics simulations showing the number of hydrogen bonds formed during the simulation period for the GLXC-25691 (control), Molport-047-717-902, Molport-010-716-199, Molport-020-263-494, Molport-005-022-518, and MolPort-007-806-063.

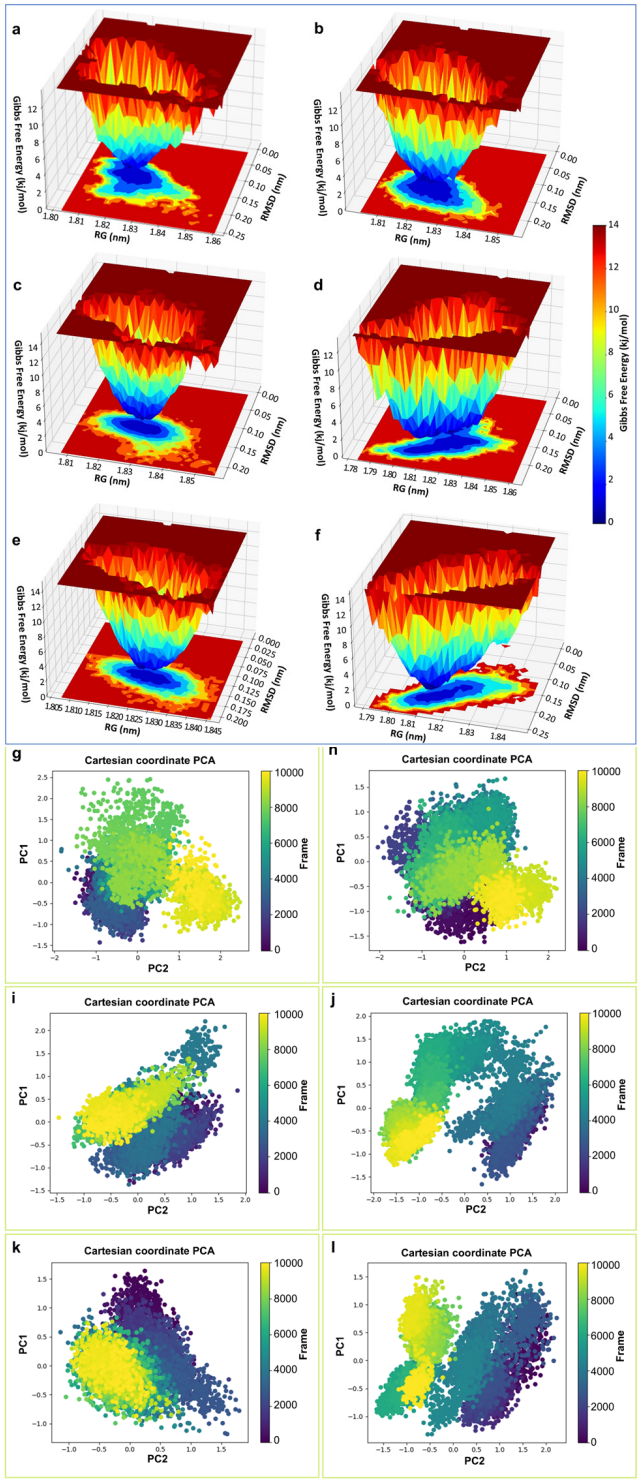

Fig. 4. Results of the molecular dynamics simulations showing the free energy landscapes for GLXC-25691 (a), Molport-047-717-902 (b), Molport-010-716-199 (c), Molport-020-263-494 (d), Molport-005-022-518 (e), and MolPort-007-806-063 (f) along with the corresponding principal component analysis (PCA) plots for GLXC-25691 (g), Molport-047-717-902 (h), Molport-010-716-199 (i), Molport-020-263-494 (j) Molport-005-022-518 (k), and MolPort-007-806-063 (l).

they maintain overall stability, likely contributing to strong binding interactions. However, Molport-047-717-902 and Molport-005-022-518 display more compact clustering, reflecting a more restricted and stable conformational space. These ligands appear to lock the protein into a more defined conformation, reducing flexibility and promoting strong, stable binding. In contrast, Molport-020-263-494 shows a broader distribution of conformational states, indicating greater flexibility and variability in the protein-ligand interaction. This increased flexibility may correlate with weaker binding, as the ligand induces less defined structural stability.

3.3.8. Molecular mechanics/generalised Born surface area (MM/GBSA) analysis

Table 1 presents the MM/GBSA analysis of screened ligands, including the control GLXC-25691. The control shows the strongest van der Waals interactions at -66.44 kcal/mol, closely followed by Molport-007-806-063 (-65.31 kcal/mol) and Molport-005-022-518 (-65.05 kcal/mol). Molport-007-806-063 exhibits the most favorable electrostatic contribution (-20.91 kcal/mol), while Molport-047-717-902 has the highest polar solvation penalty (39.98 kcal/mol). Non-polar solvation energy is similar across all ligands. In terms of gas-phase free energy, Molport-007-806-063 has the strongest interactions (-86.21 kcal/mol), while Molport-047-717-902 shows the highest desolvation penalty (32.93 kcal/mol). Overall, Molport-007-806-063 has the most favorable total binding free energy (-59.9 kcal/mol), surpassing the control (-56.26 kcal/mol). Molport-005-022-518 and Molport-010-716-199 also exhibit appreciable binding with the MAGL protein. However, Molport-020-263-494 has the lowest interaction affinity (-36.23 kcal/mol) because it has weaker van der Waals forces and higher desolvation penalties.

The overall analysis of the energy decomposition plots reveals that key hydrophobic residues, such as Leu148, Leu184, Tyr194, and Leu205, consistently play a vital role in stabilizing ligand interactions with MAGL across all complexes (Fig. 5). Ligands that exhibit strong, negative

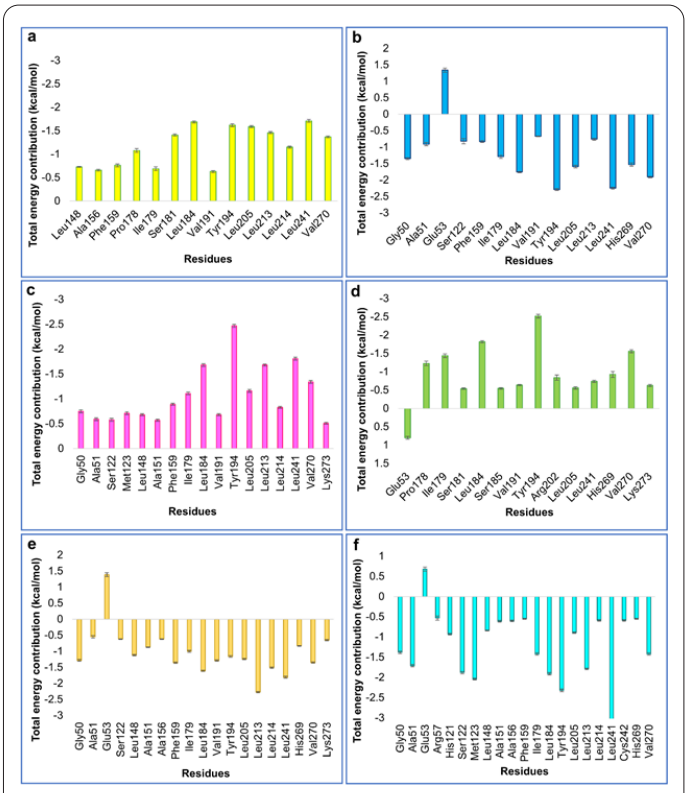

Fig. 5. Results of energy decomposition computed by molecular mechanics/general born surface area for (a) GLXC-25691 (control), (b) Molport-047-717-902, (c) Molport-010-716-199, (d) Molport-020-263-494, (e) Molport-005-022-518, and (f) MolPort-007-806-063.

Table 1. Results of molecular mechanics/general born surface area for the top five hits along with native inhibitor.

Parameters	Molport-047-717-902	Molport-010-716-199	Molport-020-263-494	Molport-005-022-518	MolPort-007-806-063	GLXC-25691 (control)
ΔE_{vdW}	-56.51±0.2	-62.45±0.2	-49.85±0.26	-65.05±0.18	-65.31±0.18	-66.44±0.23
ΔE_{ele}	-17.55±0.33	-7.49±0.28	-7.07±0.42	-8.67±0.17	-20.91±0.18	-6.59±0.11
ΔE_{gb}	39.98±0.22	23.32±0.2	26.9±0.35	28.25±0.2	34.56±0.14	24.88±0.13
ΔE_{surf}	-7.04±0.02	-7.95±0.02	-6.21±0.04	-8.11±0.02	-8.24±0.01	-8.11±0.02
ΔG_{gas}	-74.06±0.42	-69.94±0.39	-56.92±0.6	-73.72±0.25	-86.21±0.25	-73.03±0.26
ΔG_{solv}	32.93±0.22	15.37±0.19	20.69±0.32	20.14±0.2	26.32±0.14	16.77±0.12
ΔG_{Tota}	-41.13±0.33	-54.57±0.26	-36.23±0.36	-53.57±0.24	-59.9±0.23	-56.26±0.22

energy contributions from these residues, such as Molport-007-806-063 and the control, tend to have stronger binding affinities. These hydrophobic interactions provide significant stability to the complexes, explaining the higher binding free energies observed in the MM/GBSA analysis.

Molport-007-806-063 demonstrates the strongest interaction profile, with multiple key residues significantly contributing to the binding energy, especially via van der Waals interactions in hydrophobic areas, hence designating it as the ligand with the greatest overall binding affinity. Other ligands, such as Molport-010-716-199 and Molport-005-022-518, also show favorable interaction profiles, with contributions from the same key residues, though to a slightly lesser extent compared to Molport-007-806-063. These ligands still form stable interactions but do not reach the same binding efficiency. In contrast, Molport-020-263-494 and Molport-047-717-902 display a more varied interaction profile, with some residues showing weaker or even positive contributions to the total energy. This suggests less favorable interactions, leading to weaker overall binding affinities in comparison to the more tightly bound complexes.

3.4. Density functional theory (DFT) computations

The density functional theory (DFT) computations provided key insights into the electronic structure of the five ligands, particularly through analysis of their HOMO-LUMO energy gaps (ΔE). The energy gaps range from 4.32 eV to 4.75 eV, reflecting the stability and reactivity of each ligand. Molport-010-716-199 displays the largest energy gap of 4.75 eV, indicating a high degree of stability and low reactivity. This suggests that the ligand may have limited potential for strong electrostatic interactions or hydrogen bonding, as its electron-donating and -accepting capabilities are reduced. Instead, the binding interactions for this ligand are likely dominated by van der Waals forces, where weaker but stable hydrophobic interactions with the protein play a major role.

On the other hand, Molport-020-263-494, with a smaller HOMO-LUMO gap of 4.32 eV, suggests a higher reactivity, which could enable more dynamic interactions with the protein. Despite this, its overall binding affinity appears lower due to less favorable solvation, weaker van der Waals interactions, and suboptimal electrostatic contributions. This indicates that while electronic reactivity, inferred from the HOMO-LUMO gap, can facilitate interactions, it must be complemented by strong non-covalent interactions and favorable solvation properties to result in high binding affinity.

The electron density distributions across the ligands, as indicated in Fig. 6, reveal well-defined regions of positive (HOMO) and negative (LUMO) charge densities. These distributions are critical for guiding future drug design optimization. The red HOMO regions often concentrated on nitrogen atoms or aromatic systems, are key for forming electrostatic interactions with protein residues. Meanwhile, the yellow LUMO regions highlight areas where the ligands can interact with electron-rich amino acids in the protein. These features make the ligands promising candidates for further drug discovery efforts, as optimizing these electronic properties could enhance both binding affinity and specificity for their protein targets [34].

4. Discussion

This study employed a comprehensive computational approach to find potential MAGL inhibitor candidates. The pharmacophore-based approach prioritized molecules that possess key spatial and chemical properties necessary for effective MAGL binding. Drug-likeness and bioavailability filters like Lipinski's and Veber's rules efficiently eliminated unsuitable compounds early in the process. Additional steps like energy minimization and structural alignment (RMSD) were needed to narrow down the candidate list to molecules expected to bind strongly and stably. Using the single conformer and Durrant lab filters made the final candidates better by ensuring they were stable and removing possible problems like steric clashes or instability. Ultimately, molecular docking prioritized the compounds with the highest predicted binding affinity, facilitating the selection of the most promising candidates for rigorous MD simulation analysis.

The analysis of ligand-protein interactions highlighted the key residues and interaction types important for binding affinity and specificity. Consistent hydrogen bonding, hydrophobic interactions, and π-π stacking identified in top ligands provide insights into the molecular basis of MAGL inhibition. The detailed interaction profile serves as a valuable guide for further optimization and designing molecules with enhanced therapeutic potential.

Stability analysis from RMSD, RMSF, Rg, SASA, Gibbs FEL, and PCA further supported the reliability of these interactions, confirming the structural integrity and stability of ligand-MAGL complexes. The different patterns of hydrogen bonds and PCA clustering indicate that there are various ways the ligands can bind, with some ligands allowing for movement while still being stable, and

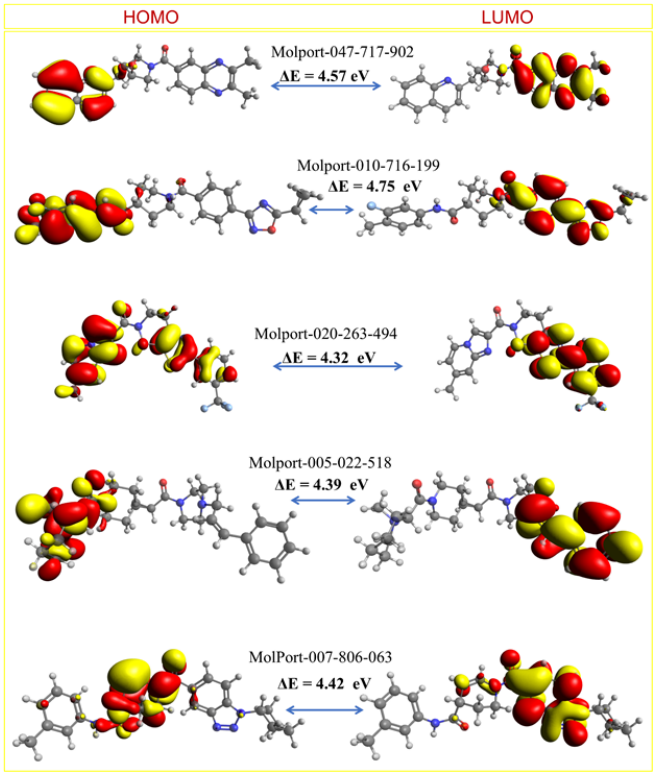

Fig. 6. Results of density functional theory computations show the highest occupied molecule orbital (HOMO) and the lowest un-occupied molecular orbital (LUMO) for the top five hits, along with the native inhibitor.

others limiting movement to improve stability. Detailed MM/GBSA and residue-level decomposition analyses uncovered critical interactions underpinning strong ligand binding, emphasizing the importance of hydrophobic residues and van der Waals forces in mediating high-affinity interactions. Complementary DFT analyses improved our understanding by linking electronic structures to binding behaviors, clearly showing how small changes in electronic properties greatly affected the strength of interactions. Studies of electron density mapping provided explicit, actionable insights, pinpointing precise structural features for future ligand optimization strategies. These insights are valuable for future ligand optimization strategies aimed at enhancing binding stability and therapeutic efficacy.

A robust pharmacophore-based virtual screening approach was employed to identify potential MAGL inhibitors in this study. Initially, a pharmacophore model was developed based on the X-ray crystal structure of MAGL complexed with its known inhibitor, (2-cyclohexyl-1,3-benzoxazol-6-yl){3-[4-(pyrimidin-2-yl)piperazin-1-yl] azetidin-1-yl}methanone. Utilizing the Pharmit web server, 5.241 million compounds from the MolPort database underwent virtual screening. The pharmacophore shape filter initially identified 28,873 compounds as potential hits. Subsequently, the application of Lipinski's and Veber's rules narrowed the candidate pool down to 11,366 compounds. Further refinement using an energy cutoff of -7.0 kcal/mol computed by the integrated Smina module in Pharmit reduced this number to 10,198 hits. An additional filter employing a minimized RMSD cutoff of 2 Å ensured consistency of predicted binding poses with the initial pharmacophore query-aligned conformation after energy minimization, narrowing the results further to 5,771 hits. After filtering for single conformers, the number of compounds decreased to 4,156. A subsequent Durrant Lab filter further reduced the dataset to 4,027 compounds by removing substructures that, while technically feasible, are improbable or otherwise unsuitable for virtual screening. These 4,027 filtered hits were docked using Vina-GPU, and the five highest-ranking compounds were selected for detailed analysis.

In-depth computational assessments, including DFT calculations, MD simulations, and MMGBSA analyses, were performed. MMGBSA computations highlighted MolPort-007-806-063 as the most promising candidate, displaying the strongest binding energy of -59.9 ± 0.23 kcal/mol, surpassing even the reference co-crystal inhibitor, which showed a binding energy of -56.26 ± 0.22 kcal/mol. The other top candidates demonstrated binding energies of -54.57 ± 0.26 kcal/mol, -53.57 ± 0.24 kcal/mol, -41.13 ± 0.33 kcal/mol, and -36.23 ± 0.36 kcal/mol, respectively. Additionally, detailed per-residue interaction analyses were conducted to further elucidate binding interactions. Collectively, these findings indicate that MolPort-007-806-063 and the other top-ranking candidates represent promising leads for future experimental validation and potential therapeutic development as novel MAGL inhibitors. Suggested experimental validations include enzyme inhibition assays, cell-based activity assays, and crystallographic studies to confirm the binding modes and potency predicted by these computational analyses.

Conflict of interests

The author has no conflicts with any step of the article preparation.

Consent for publications

The author read and approved the final manuscript for publication.

Ethics approval and consent to participate

No human or animals were used in the present research.

Informed consent

The authors declare that no patients were used in this study.

Availability of data and material

The data that support the findings of this study are available from the corresponding author upon reasonable request.

Authors' contributions

Faizul Azam: Conceptualization, methodology, investigation, data curation, software, validation, Writing-original draft, supervision, funding acquisition and writing-review & editing.

Acknowledgments

The author gratefully acknowledges Qassim University, represented by the Deanship of Graduate Studies and Scientific Research, on the financial support for this research under the number (2023-SDG-1-HMSRC-36541) during the academic year 1445 AH /2023 AD.

References

1. Min H-Y, Lee H-Y (2022) Molecular targeted therapy for anticancer treatment. Exp Mol Med 54:1670–1694. https://doi.org/10.1038/s12276-022-00864-3
2. Nussinov R, Tsai C-J, Jang H (2021) Anticancer drug resistance: An update and perspective. Drug Resist Updat 59:100796. https://doi.org/10.1016/j.drup.2021.100796
3. Nass SJ, Rothenberg ML, Pentz R, et al (2018) Accelerating anticancer drug development — opportunities and trade-offs. Nat Rev Clin Oncol 15:777–786. https://doi.org/10.1038/s41571-018-0102-3
4. He Y, Krämer SD, Grether U, et al (2024) Identification of (R)-[18 F]YH134 for Monoacylglycerol Lipase Neuroimaging and Exploration of Its Use for Central Nervous System and Peripheral Drug Development. J Nucl Med 65:300–305. https://doi.org/10.2967/jnumed.123.266426
5. Ren S-Y, Wang Z-Z, Zhang Y, Chen N-H (2020) Potential application of endocannabinoid system agents in neuropsychiatric and neurodegenerative diseases—focusing on FAAH/MAGL inhibitors. Acta Pharmacol Sin 41:1263–1271. https://doi.org/10.1038/s41401-020-0385-7
6. Nomura DK, Long JZ, Niessen S, et al (2010) Monoacylglycerol Lipase Regulates a Fatty Acid Network that Promotes Cancer Pathogenesis. Cell 140:49–61. https://doi.org/10.1016/j.cell.2009.11.027
7. Qin H, Ruan Z (2014) The Role of Monoacylglycerol Lipase (MAGL) in the Cancer Progress. Cell Biochem Biophys 70:33–36. https://doi.org/10.1007/s12013-014-9899-2
8. Chen T, Li H (2017) Fatty acid metabolism and prospects for targeted therapy of cancer. Eur J Lipid Sci Technol 119:1600366. https://doi.org/10.1002/ejlt.201600366
9. Deng H, Li W (2020) Monoacylglycerol lipase inhibitors: modulators for lipid metabolism in cancer malignancy, neurological and metabolic disorders. Acta Pharm Sin B 10:582–602. https://

doi.org/10.1016/j.apsb.2019.10.006
10. Wang C, Li Z, Zhong L, Chen Y (2022) Inhibition of monoacylglycerol lipase restrains proliferation, migration, invasion, tumor growth and induces apoptosis in cervical cancer. J Obstet Gynaecol Res 48:456–466. https://doi.org/10.1111/jog.15110
11. Prüser JL, Ramer R, Wittig F, et al (2021) The Monoacylglycerol Lipase Inhibitor JZL184 Inhibits Lung Cancer Cell Invasion and Metastasis via the CB1 Cannabinoid Receptor. Mol Cancer Ther 20:787–802. https://doi.org/10.1158/1535-7163.MCT-20-0589
12. MA M, BAI J, LING Y, et al (2016) Monoacylglycerol lipase inhibitor JZL184 regulates apoptosis and migration of colorectal cancer cells. Mol Med Rep 13:2850–2856. https://doi.org/10.3892/mmr.2016.4829
13. Aghazadeh Tabrizi M, Baraldi PG, Baraldi S, et al (2018) Discovery of 1,5-Diphenylpyrazole-3-Carboxamide Derivatives as Potent, Reversible, and Selective Monoacylglycerol Lipase (MAGL) Inhibitors. J Med Chem 61:1340–1354. https://doi.org/10.1021/acs.jmedchem.7b01845
14. Granchi C, Lapillo M, Glasmacher S, et al (2019) Optimization of a Benzoylpiperidine Class Identifies a Highly Potent and Selective Reversible Monoacylglycerol Lipase (MAGL) Inhibitor. J Med Chem 62:1932–1958. https://doi.org/10.1021/acs.jmedchem.8b01483
15. Wu Z, Chen S, Wang Y, et al (2024) Current perspectives and trend of computer-aided drug design: a review and bibliometric analysis. Int J Surg 110:3848–3878. https://doi.org/10.1097/JS9.0000000000001289
16. Lavecchia A, Giovanni C (2013) Virtual Screening Strategies in Drug Discovery: A Critical Review. Curr Med Chem 20:2839–2860. https://doi.org/10.2174/09298673113209990001
17. Tuccinardi T (2021) What is the current value of MM/PBSA and MM/GBSA methods in drug discovery? Expert Opin Drug Discov 16:1233–1237. https://doi.org/10.1080/17460441.2021.1942836
18. Wang E, Sun H, Wang J, et al (2019) End-Point Binding Free Energy Calculation with MM/PBSA and MM/GBSA: Strategies and Applications in Drug Design. Chem Rev 119:9478–9508. https://doi.org/10.1021/acs.chemrev.9b00055
19. Sunseri J, Koes DR (2016) Pharmit: interactive exploration of chemical space. Nucleic Acids Res 44:W442–W448. https://doi.org/10.1093/nar/gkw287
20. Lipinski CA, Lombardo F, Dominy BW, Feeney PJ (2001) Experimental and computational approaches to estimate solubility and permeability in drug discovery and development settings. Adv Drug Deliv Rev 46:3–26. https://doi.org/10.1016/s0169-409x(00)00129-0
21. Veber DF, Johnson SR, Cheng H-Y, et al (2002) Molecular properties that influence the oral bioavailability of drug candidates. J Med Chem 45:2615–2623. https://doi.org/10.1021/jm020017n
22. Ali A, Ali A, Warsi MH, et al (2022) Toward the Discovery of a Novel Class of Leads for High Altitude Disorders by Virtual Screening and Molecular Dynamics Approaches Targeting Carbonic Anhydrase. Int. J. Mol. Sci. 23
23. Ropp PJ, Spiegel JO, Walker JL, et al (2019) Gypsum-DL: an open-source program for preparing small-molecule libraries for structure-based virtual screening. J Cheminform 11:34. https://doi.org/10.1186/s13321-019-0358-3
24. O'Boyle NM, Banck M, James CA, et al (2011) Open Babel: An open chemical toolbox. J Cheminform 3:33. https://doi.org/10.1186/1758-2946-3-33
25. Ding J, Tang S, Mei Z, et al (2023) Vina-GPU 2.0: Further Accelerating AutoDock Vina and Its Derivatives with Graphics Processing Units. J Chem Inf Model 63:1982–1998. https://doi.org/10.1021/acs.jcim.2c01504
26. Trott O, Olson AJ (2010) AutoDock Vina: improving the speed and accuracy of docking with a new scoring function, efficient optimization, and multithreading. J Comput Chem 31:455–461
27. Schalk-Hihi C, Schubert C, Alexander R, et al (2011) Crystal structure of a soluble form of human monoglyceride lipase in complex with an inhibitor at 1.35 Å resolution. Protein Sci 20:670–683. https://doi.org/10.1002/pro.596
28. Abraham MJ, Murtola T, Schulz R, et al (2015) GROMACS: High performance molecular simulations through multi-level parallelism from laptops to supercomputers. SoftwareX 1–2:19–25. https://doi.org/10.1016/j.softx.2015.06.001
29. Valdés-Tresanco MS, Valdés-Tresanco ME, Valiente PA, Moreno E (2021) gmx_MMPBSA: A New Tool to Perform End-State Free Energy Calculations with GROMACS. J Chem Theory Comput 17:6281–6291. https://doi.org/10.1021/acs.jctc.1c00645
30. Singh G, Al-Fahad D, Al-Zrkani MK, et al (2023) Identification of potential inhibitors of HER2 targeting breast cancer—a structure-based drug design approach. J Biomol Struct Dyn 1–18. https://doi.org/10.1080/07391102.2023.2246576
31. Neese F (2018) Software update: the ORCA program system, version 4.0. WIREs Comput Mol Sci 8:e1327. https://doi.org/10.1002/wcms.1327
32. Becke AD (1988) Density-functional exchange-energy approximation with correct asymptotic behavior. Phys Rev A 38:3098–3100. https://doi.org/10.1103/PhysRevA.38.3098
33. Lee C, Yang W, Parr RG (1988) Development of the Colle-Salvetti correlation-energy formula into a functional of the electron density. Phys Rev B 37:785–789. https://doi.org/10.1103/PhysRevB.37.785
34. De B, Bhandari K, Mendonça FJB, et al (2019) Computational Studies in Drug Design Against Cancer. Anticancer Agents Med Chem 19:587–591. https://doi.org/10.2174/1871520618666180911125700